International Journal of Electronics, Electrical and Computational System
IJEECS
ISSN 2348-117X
Volume 6, Issue 7
July 2017

Academic Science

Steady State Analysis of Interleaved High Conversion Ratio Bidirectional DC-DC Converter

Aruna Sri Harika
Gudlavalleru Engineering College,
Gudlavalleru.,A.P, India

Vargil Kumar
Gudlavalleru Engineering College,
Gudlavalleru.,A.P, India.,

ABSTRACT- A bidirectional dc to dc converter is necessary between the energy storage battery and the supply to match the voltage level. For high to low power range application bidirectional isolated converter is proposed for induction motor drive. The isolated bidirectional converter is operated in both step down and step up modes. In this work, Bidirectional Isolated converter is designed to operate with high conversion ratio and high efficiency. By using a voltage doubler circuit in high voltage side increases the conversion ratio.Bidirectional converters allow transfer of power between two dc sources, in either direction. Due to their ability to reverse the direction of flow of current, and thereby power, while maintaining the voltage polarity at either end unchanged, they are beneficial when use in applications like, battery charger circuits,bidirectional converters may be isolated type or non-isolated type. High voltage conversion ratio in bidirectional converters is able to be achieved easily by adjusting turns ratio of the isolated transformer. The bidirectional fly back converter is a simple and low-cost, distributed energy storage systems can be well conjugated and integrated to realize power distribution between energy generation systems and storage systems by bidirectional converters (BDCs). Then, the evolution of the proposed extensible topologies and the steady-state operating principle under the inductor current continuous conduction mode is presented.

KEY WORDS*: **Bidirectional dc–dc converter (BDC), coupled inductor (CI), high conversion ratio, interleaved, switched capacitor(SC), Induction motor drive.***

I. INTRODUCTION

Sources of electric energy for industry, agriculture, civilian or military use differ in their purposes, appliance and supplied system types. Autonomous generation systems, sources based on solar and wind energy, are commonly used to supply various appliances, facilities, systems, and provide for heating, illumination, and other purposes in almost all spheres. Almost all of these systems use super-capacitors, accumulators (batteries) or different energy buffers for stable operation under all possible conditions and requirements.

For the reason above and due to the growing needs in systems with the ability of bidirectional energy transmission between two dc buses, Bidirectional DC-DC Converters (BDCs) have received increased attention.

Apart from their traditional application in energy storage and dc motor drives, BDCs have become a promising option for many applications, such as portable devices, spacecraft power systems, Uninterruptible Power Supplies (UPS), electric vehicles [1], fuel cells and renewable energy systems [2], [3].

In the electric vehicle application, an auxiliary energy storage battery absorbs the energy fed back by the electric machine during deceleration of the motors. In addition, BDC is also required for the power supply from auxiliary battery to boost the high-voltage bus during motor startup or acceleration when a large amount of power is required [1], [4]-[7]. Moreover, BDCs can also be used in industrial equipment. Such equipment started and stopped very frequently, so energy can be recuperated without being wasted.

International Journal of Electronics, Electrical and Computational System
IJEECS
ISSN 2348-117X
Volume 6, Issue 7
July 2017

Academic Science

Recently, clean energy resources such as solar photovoltaic technologies and wind turbines have been widely exploited for developing renewable power generation systems. However, fluctuations of power generation due to changes in weather conditions and occasional massive needs in output power makes Renewable Energy Sources (RES) inapplicable for selfcontained operation as the single power source. The typical solution to this problem is the use of energy storage devices in conjunction with the RES to compensate this variability and obtain a stable and smooth power flow to the load. The most applicable and cost-effective energy storage devices in the medium-power range are lithium-ion or other types of batteries and super-capacitors. A renewable power system with BDC is shown in BDCs maintain a stable load bus voltage and make full usage of the solar array, wind turbine, fuel cell and the storage battery in all operating modes [7]-[13]. This paper proposes a general classification of bidirectional DC-DC Converter.A typical dc microgrid system is shown in Fig.1. Multiple distributed renewable energy resources, energy-storage devices, and dc loads are connected to a 380-V dc bus (380 to 800 V) using different power converters. To make such systems distributed and reliable, energy-storage devices are adopted to smooth the dc bus voltage waveform and output power, improve the dynamic response, and guarantee the stability of the system [14-15].

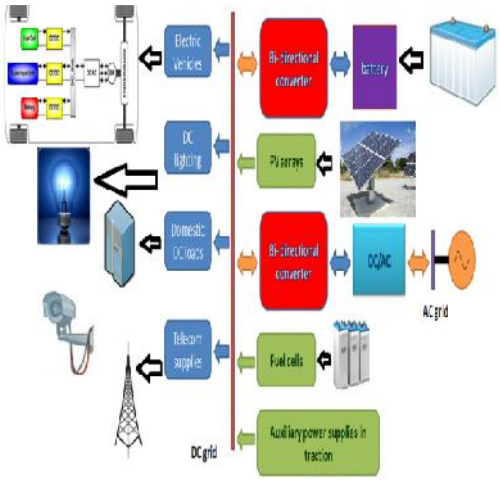

Fig.1. Typical block diagram of a dc microgrid system.

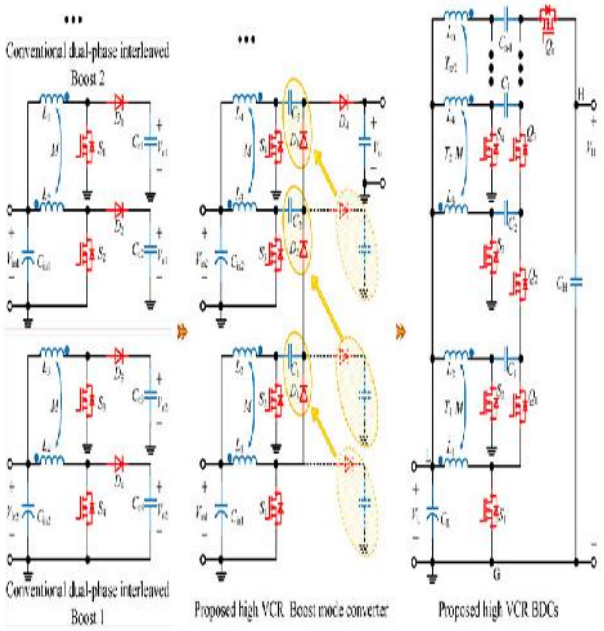

Fig.2. Evolution of the proposed extensible topologies

II. POWER STAGE DESCRIPTION AND OPERATING PRINCIPLES

A. Proposed Topologies

The evolution procedure and general structure of the proposed multiphase SC-BDCs are shown in Fig.2. V_L represents the low dc-link voltage of the parallel-connected battery arrays, while V_H represents the high-voltage port of the dc bus. In this paper, the four-phase case is studied, as shown in Fig.3. It consists of four phases: phase 1 (L_1 S_1 Q_1), phase 2 (L_2 S_2 C_1 Q_2), phase 3(L_3 S_3 C_2 Q_3), and phase 4 (L_4 S_4 C_3 Q_4). Phases 1 and 2 share an inverse CI with a turn ratio of N = 1:1 and a coupling coefficient denoted by k ($0 < k < 1$); the case of phases 3 and 4 is similar. The use of CIs can reduce inductance and mitigate channel ripple current effectively. Furthermore, the input current can share ACS among four parallel inductors because of the existence of the SCs and the volt–second balance principle. Phases 1 and 3 (or phases 2 and 4) share the synchronous gate pulse width modulation (PWM) signal; moreover, phases 1 and 2 (or phases 3 and 4) share the complementary PWM signal. When the circuit is at the boost stage, energy flows from V_L to V_H, and the duty cycle of gate drive signals D_B for S_1, S_2, S_3, and S_4 (forward MOSFETs) should be higher than 0.5 to eliminate

International Journal of Electronics, Electrical and Computational System
IJEECS
ISSN 2348-117X
Volume 6, Issue 7
July 2017

circulating current during the turn-off period of all the ground connected MOSFETs. Q_1, Q_2, Q_3, and Q_4 (SRMOSFETs) will be working in synchronous rectification (SR) mode. Conversely, when the circuit is at the buck stage, energy flows from V_H to V_L; the duty cycle of gate drive signals D_K for Q_1, Q_2, Q_3, and Q_4 should be less than 0.5; and S_1, S_2, S_3, and S_4 will be working in SR mode.

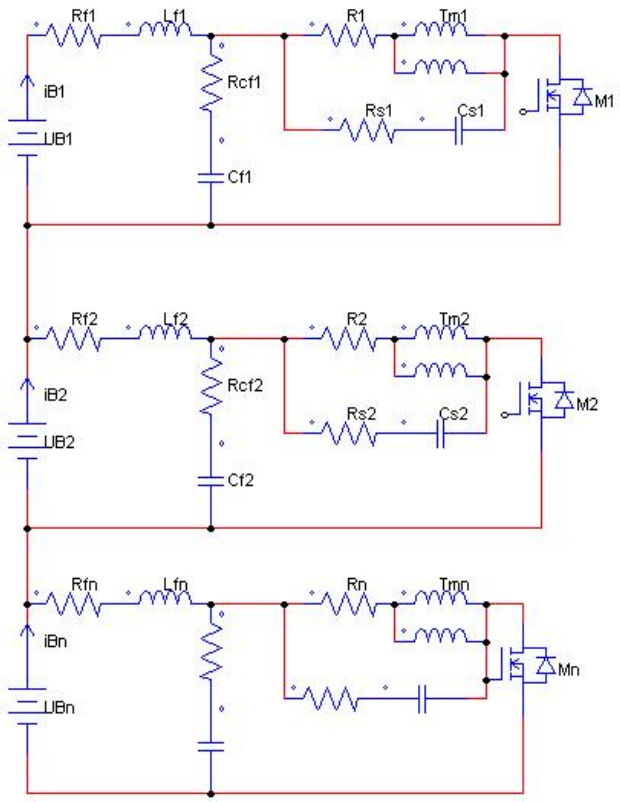

Fig.3. Schematic of the proposed four-phase high VCR BDC.

Because of circuit symmetry, the component parameters are designed identically to simplify circuit analyses and prototype construction: Initial inductanceL1 =L2 =L3 =L4 =L, with the coupling coefficient k; and the mutual inductances M of each CI are equal, i.e., k=M/L; capacitance C1 =C2 =C3.For steady-state analysis, two more assumptions are included as follows:

1) All switches are regarded as ideal.

2) C1, C2, and C3 are large enough that VC1, VC2, and VC3 can be considered to be constants during one switching period.

B. Operation Principles at the Boost Stage of Continuous Current Mode (CCM)

Fig.4 shows the major operating waveforms of the proposed high VCR BDC at the CCM boost stage and Fig.5 shows the equivalent circuits after inductor decoupling. The CIs, L_1 and L_2, can be represented by an equivalent circuit with three uncoupled inductors: the mutual inductance − M_1, and the equivalent leakage inductances, $L_1 + M_1$ and $L_2 + M_1$. In the same way, L_3 and L_4 can be replaced by − M_2, $L_3 + M_2$, and $L_4 + M_2$. Consequently, the voltages v_{L1}, v_{L2}, v_{L3}, and v_{L4} of L_1, L_2, L_3, and L_4 can be obtained

$$V_{L1} = V_{L1+M1} + V_{-M1}$$
$$V_{L2} = V_{L2+M1} + V_{-M1}$$
$$V_{L3} = V_{L3+M2} + V_{-M2}$$
$$V_{L4} = V_{L4+M2} + V_{-M2} \quad (1)$$

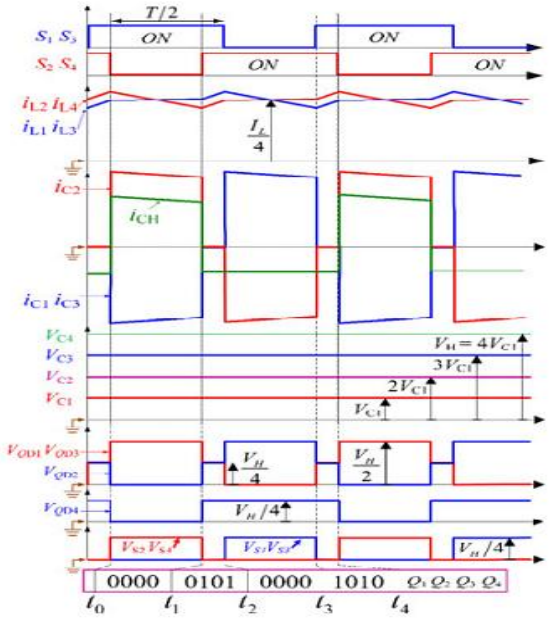

Fig.4. Operating waveforms at the CCM boost stage.

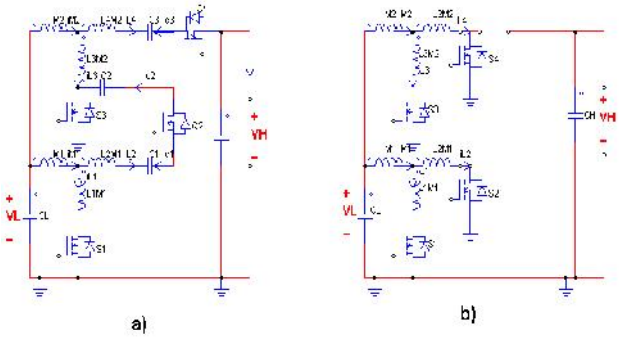

International Journal of Electronics, Electrical and Computational System
IJEECS
ISSN 2348-117X
Volume 6, Issue 7
July 2017

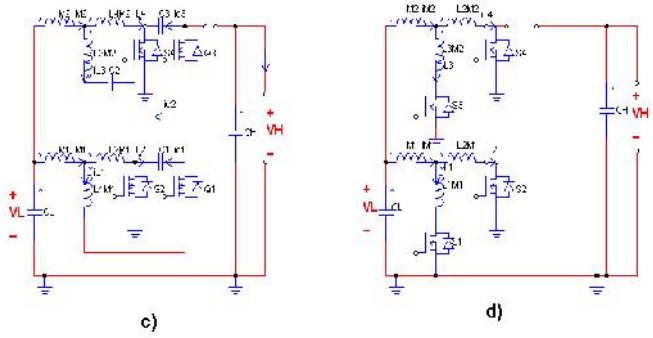

Fig.5. Equivalent circuits at the CCM boost stage. (a) Mode 1. (b) Mode 2. (c) Mode 3. (d) Mode 4.

Mode 1 [$t_0 - t_1$]: S_1 and S_3 are ON, while S_2 and S_4 are turned OFF. $L_1 + M_1$ and $-M_1$ are charged by V_L. Meanwhile, $L_2 + M_1$ and $-M_1$ are series connected with C_1 to charge C_2. $L_3 + M_2$ and $-M_2$ are charged by V_L; and $L_4 + M_2$, $-M_2$, and C_3 are series connected to charge capacitor C_H and the load. The voltage equations across the inductors can be obtained from Kirchhoff's voltage law

$$L_1 \cdot di_{L1}/dt - M.di_{L2}/dt = V_L = V_{L1}$$
$$L_2 \cdot di_{L2}/dt - M.di_{L1}/dt = V_L + Vc_1 - Vc_2 = V_{L2}$$
$$L_3 \cdot di_{L3}/dt - M.di_{L4}/dt = V_L = V_{L3}$$
$$L_4 \cdot di_{L4}/dt - M.di_{L3}/dt = V_L + Vc_3 - V_H = V_{L4} \quad (2)$$

The SC charge/discharge currents are exactly equal to the inductor currents: $i_{C1} = -i_{L2}$, $i_{C2} = i_{L2}$, and $i_{C3} = -i_{L4}$. Therefore, soft charging proposed in [52] and [53] is achieved, and surge currents during charging and discharging can be avoided.

Mode 2 [$t_1 - t_2$]: S_1, S_2, S_3, and S_4 are turned ON, and Q_1, Q_2, Q_3, and Q_4 are OFF. $L_1 + M_1$, $L_2 + M_1$, and $-M_1$ are charged by V_L. Meanwhile, $L_3 + M_2$, $L_4 + M_2$, and $-M_2$ are charged by V_L through S_3 and S_4, and the load absorbs energy from CH. The voltages across the SCs remain constant. The voltage equations of the inductors can be presented as follows:

$$V_{L1} = V_L = L_1 \cdot di_{L1}/dt - M.di_{L2}/dt$$
$$V_{L2} = V_L = L_2 \cdot di_{L2}/dt - M.di_{L1}/dt$$
$$V_{L3} = V_L = L_3 \cdot di_{L3}/dt - M.di_{L4}/dt$$
$$V_{L4} = V_L = L_4 \cdot di_{L4}/dt - M.di_{L3}/dt \quad (3)$$

Mode 3 [$t_2 - t_3$]: S_1 and S_3 are turned OFF, and Q_1 and Q_3 begin conducting; whereas S_2 and S_4 are ON, and Q_2 and Q_4 are turned OFF. $L_1 + M_1$ and $-M_1$ release energy to C_1 through Q_1; and $L_2 + M_1$ is charged through V_L, $-M_1$, and S_2. The total current $-M_1$ ($= i_{L1} + i_{L2}$) flowing through $-M_1$ goes down linearly so that $-M_1$ releases energy. Similarly, series connected $L_3 + M_2$, $-M_2$, V_L, and C_2 charge energy to C_3 through Q_3. $L_4 + M_2$ and $-M_2$ are linearly charged by V_L, $-M_2$ releases energy due to the decreasing total current $-M_2$ ($= i_{L3} + i_{L4}$). Also, $i_{C1} = i_{L1}$, $i_{C2} = -i_{L3}$, and $i_{C3} = i_{L3}$. The voltage across L_1, L_2, L_3, and L_4 can be listed as follows:

$$L_1 \cdot di_{L1}/dt - M.di_{L2}/dt = V_L - Vc_1 = V_{L1}$$
$$L_2 \cdot di_{L2}/dt - M.di_{L1}/dt = V_L = V_{L2}$$
$$L_3 \cdot di_{L3}/dt - M.di_{L4}/dt = V_L + Vc_2 - Vc_3 = V_{L3}$$
$$L_4 \cdot di_{L4}/dt - M.di_{L3}/dt = V_L = V_{L4} \quad (4)$$

Mode 4 [$t_3 - t_4$]: This is the same as Mode 2. S_1, S_2, S_3, and S_4 are all ON, and Q_1, Q_2, Q_3, and Q_4 are switched OFF; $L_1 + M_1$, $L_2 + M_1$, $L_3 + M_2$, $L_4 + M_2$, $-M_1$, and $-M_2$ are all linearly charged by V_L.

In buck mode, the operation of the circuit is the same, but with reversed power flow.

III. FEATURE ANALYSIS AND COMPARISON

A. Voltage Gain and Duty Ratio

According to the steady-state analysis, and by combining equations (1)–(3), the switching equations of L_1, L_2, L_3, and L_4 can be written as follows:

$$V_{L1} = S_1 \cdot V_L + (1-S_1) \cdot (V_L - V_{C1})$$
$$V_{L2} = S_2 \cdot V_L + (1-S_2) \cdot (V_L + V_{C1} - V_{C2})$$
$$V_{L3} = S_3 \cdot V_L + (1-S_3) \cdot (V_L + V_{C2} - V_{C3})$$
$$V_{L4} = S_4 \cdot V_L + (1-S_4) \cdot (V_L + V_{C3} - V_H) \quad (5)$$

In consequence, by applying the volt–second balance principle

$$D_B \cdot V_L + (1-D_B) \cdot (V_L - V_{C1}) = 0$$
$$D_B \cdot V_L + (1-D_B) \cdot (V_L + V_{C1} - V_{C2}) = 0$$
$$D_B \cdot V_L + (1-D_B) \cdot (V_L + V_{C2} - V_{C3}) = 0$$
$$D_B \cdot V_L + (1-D_B) \cdot (V_L + V_{C3} - V_H) = 0 \quad (6)$$

From (5) and (6), the voltage gain for the proposed four-phase BDC topology at the CCM boost stage can be obtained

$$V_H = 4V_{C1}/3 = 4V_{C2}/2 = 4V_{c1} = 4V_L/(1-D_B) \quad (7)$$
$$V_H = 4V_{C1}/3 = 4V_{C2}/2 = 4V_{c1} = 4V_L/(1-D_B) \quad (8)$$

Similarly, the voltage gain at the CCM buck stage is deduced as

$$M_H = V_H/V_L = D_K/4 \quad (9)$$

DB represents the duty cycle of power switches S_1 – S_4, while DK corresponds to Q_1– Q_4. Moreover,

International Journal of Electronics, Electrical and Computational System
IJEECS
ISSN 2348-117X
Volume 6, Issue 7
July 2017

Academic Science

$S_i$and Q_i are turned ON or OFF in a mutually complementary pattern (i = 1, 2, 3, 4).

The ideal/real voltage ratio and the duty cycle of the proposed four-phase BDC, and the comparison curves with traditional boost or buck converters are sketched in Fig.14 The worst-case ESRs of each inductor and capacitor are taken as 0.2 and 0.05 Ω, respectively. The expected operation region and the rated operation point are also given in the curves.

High VCR can be implemented by either increasing the number of phases N or by increasing D_B (or decreasing D_K), and it is well known that the maximum efficiency of boost or buck converters appears when D_B or D_K is close to 0.5. Therefore, based on the design procedure proposed in [55] to optimize the design of the proposed DBC based on loss, volume, and cost optimization, guarantee the efficiency under all conditions, and avoid the effect of ESRs, the maximum D_B or minimum D_K are limited, for example D_{B-max} = 0.8or D_{K-min} = 0.25. Subsequently, the number of phases N can be calculated as shown in Fig.7; in this study, N = *4*was selected.

Another advantage is that this topology can extend the power level and VCR easily, as shown in Fig.7.

The voltage gain for the extended multiphase BDC topology at the CCM boost stage can be obtained as follows:

$$V_H = (V_{L1}\cdot N_1 + V_{L2}\cdot N_2 + \cdots\cdots + V_N\cdot N_N)/(1-D_B) \quad (10)$$

Similarly, the voltage gain at the CCM buck stage is deduced as

$$V_{Ln} = D_K V_H N_n /(N_1+N_2+\cdots+N_N),(n=1,2,3,\cdots N) \quad (11)$$

As shown in Fig.7, the multiport at LVS ensures that the proposed topologies can be applied to hybrid energy-storage systems, and the parallel cells can further reduce ripple current and voltage at HVS for high-power applications.

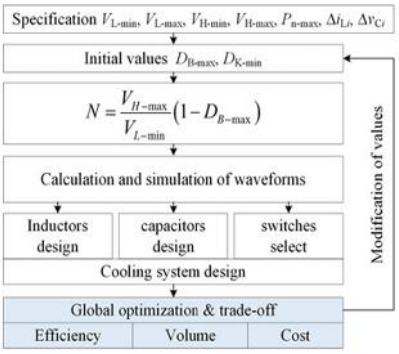

Fig.6. Flowchart of the optimization algorithm.

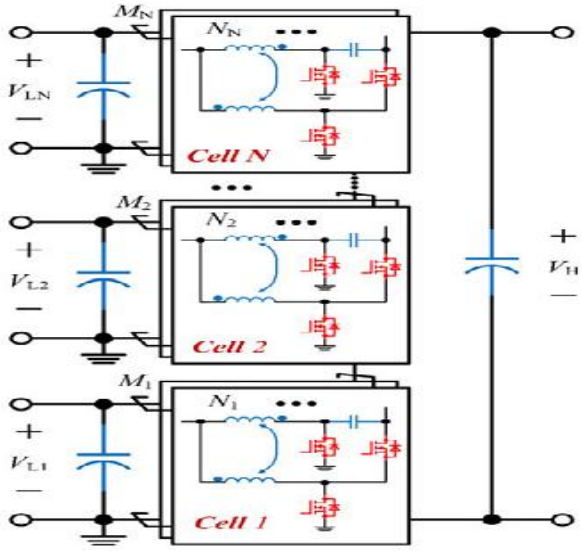

Fig.7. Extended structures of the proposed topology.

Where N_1, N_2, ...,$N_N$andM_1, M_2, ..., M_N are integers greater than 1, i.e., (2, 3, 4, . . .).

B. Voltage and Current Stresses of Power Switches

Based on the operation analysis presented, the voltage stresses on S_1– S_4 and Q_4 are $V_H/4$, while the voltage stresses on Q_1, Q_2, and Q_3 are $V_H/2$ at either the CCM boost or the CCM buck stage. Correspondingly, when the circuit is working under discontinuous current mode, all switches will suffer $V_H/2$ voltage stress. Therefore, during normal states, the voltage stresses of power switches only relate to the value of V_H rather than the duty cycle, the value of V_L, or load variations. It can be seen from Fig.6 that the voltage gain of the novel structure at the boost/buck stage is four times that of the conventional boost/buck converter, while the voltage stress is only 1/2.

The maximum current through S_2 occurs at the moment when S_1 turns OFF, and comprises two inductor currents. (The situation with S_3 and S_4 is similar.) The maximum current through S_2 can be calculated according to the following equation:

$$i_{pk\text{-}Si} = \frac{2\ n}{V_H\cdot(1-D_B)} + \frac{V_L\cdot(D_B-0.5)}{L_E\cdot f_S},\ (i = 2,3,4) \quad (12)$$

Where L_{EQ1D} is given in (13), and P_n is the rated power.

Combining (2) with (7), the voltage across inductor L_1 in Mode 1 (L_{EQ1A}) can be obtained; the equivalent

International Journal of Electronics, Electrical and Computational System
IJEECS
ISSN 2348-117X
Volume 6, Issue 7
July 2017

inductance for phase 1 in Mode 2 (L_{EQ1B}), Mode 3 (L_{EQ1C}), and Mode 4 (L_{EQ1D}) can be deduced in a similar way

$$L_{EQ1A} = \frac{L^2-M^2}{L-\alpha}$$
$$L_{EQ1B} = L-M$$
$$L_{EQ1C} = \frac{L^2-M^2}{L-\beta}$$
$$L_{EQ1D} = L-M \quad (13)$$

Similarly, the maximum current through S_1, Q_1, Q_2, Q_3, and Q_4 can be given as (3.14), where L_{EQ1C} is also given in (13)

$$i_{pk\text{-}S\,i} = i_{pk\text{-}Q} = \frac{Pn}{VH\cdot(1-DB)} + \frac{(VL-VC)\cdot(1-DB)}{2\,E\cdot fS} \quad (14)$$

C. Autocurrent Sharing

Similar to the auto energy balance of module input capacitors in the previously mentioned ISOP converter [54], the ACS mechanism of the proposed high VCR BDC is achieved based on the ampere–second balance mechanism of SCs. In theory, for static current sharing, even with different inductor values, the proposed BDCs can achieve ACS, provided that each channel operates at the same duty cycle. Based on Fig.3.4 and the analysis above, the current expressions for SCs can be presented as follows:

$$i_{c1} = (1-S_1.S_3)\cdot iL1 - (1-S_2.S_4)\cdot i_{L2}$$
$$i_{c2} = (1-S_2.S_4)\cdot iL2 - (1-S_1.S_3)\cdot i_{L3}$$
$$i_{c3} = (1-S_1.S_3)\cdot iL3 - (1-S_2.S_4)\cdot i_{L4} \quad (15)$$

Where S_1, S_2, S_3, and S_4 (with possible values of "0" or "1") are the switching states of the corresponding power switches.

$$-I_{L2\_A}\ (t_1 - t_0) + I_{L1\_C}\ (t_3 - t_2) = 0$$
$$I_{L2\_A}\ (t_1 - t_0) - I_{L3\_C}\ (t_3 - t_2) = 0$$
$$-I_{L4\_A}\ (t_1 - t_0) + I_{L3\_C}\ (t_3 - t_2) = 0 \quad (16)$$

Where I_{L1_C}, I_{L2_A}, I_{L3_C}, and I_{L4_A} represent the mean values of the corresponding inductor current during the time intervals [t_2, t_3] or [t_0, t_1]. The time period of $t_3 - t_2$ equals $t_1 - t_0$ when S_1, S_2, S_3, and S_4 have the same duty cycle D_B; therefore, $I_{L2\_A} = I_{L1\_C}$, $I_{L2\_A} = I_{L3\_C}$, and $I_{L3\_C} = I_{L4\_A}$ are obtained. Actually, the SC or CI currents during a specified time interval: I_{L1_C}, I_{L2_A}, I_{L3_C}, and I_{L4_A} are equal to the average currents of the corresponding inductors ($I_{L1} = I_{L1\_C}$, $I_{L2} = I_{L2\_A}$, $I_{L3} = I_{L1\_C}$, $I_{L4} = I_{L4\_A}$). Therefore, ACS among the inductors can be achieved if the switches S_1, S_2, S_3, and S_4 share the same turn-on duty cycle; meanwhile, soft-charging of each SC is realized.

IV. MATLAB/SIMULINK RESULTS

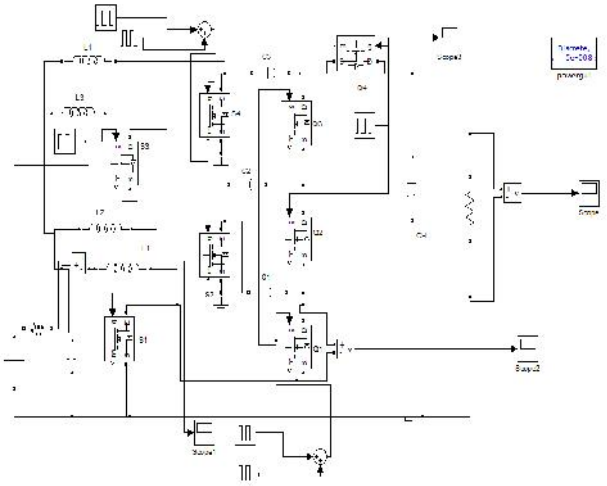

Fig.8 Simulink model of Buck converter

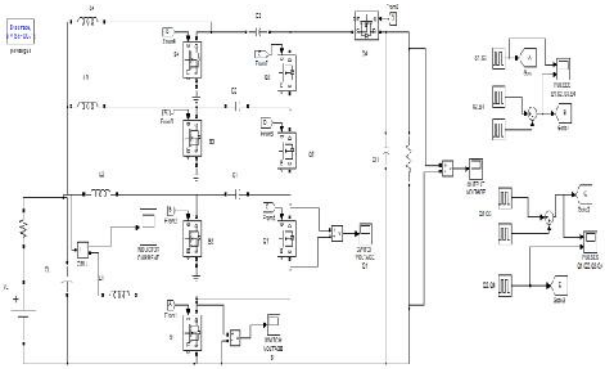

Fig.9 Simulink model of Boost converter

Table 1. Parameters of Proposed Configuration

Parameters	Values
Rated Power	1 Kw
VL, Low Voltage	24-48 V
HL High voltage	400 V
Operating Frequency	200 KHz
Switched Capacitors (C1, C2,C3)	10 µF
Input Capacitive Filter	15 µF
Output Capacitive Filter	16 µF
Inductance (L1, L2)	125.7 µH
Inductance (L3)	128.4 µH
Inductance (L4)	127.1 µH

International Journal of Electronics, Electrical and Computational System
IJEECS
ISSN 2348-117X
Volume 6, Issue 7
July 2017

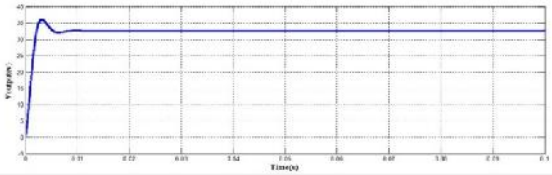

Fig.11 Buck output voltage

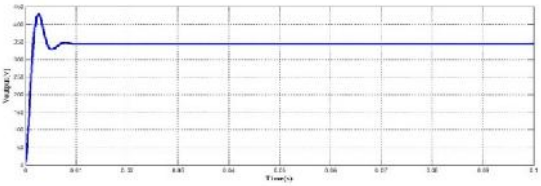

Fig.12 Boost output voltage

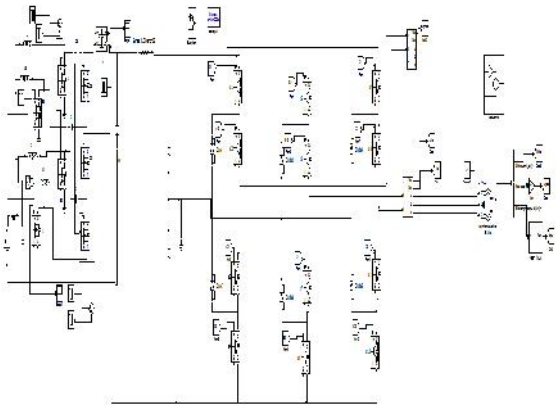

Fig.13Simulink model of Boost converter through inverter based induction motor drive

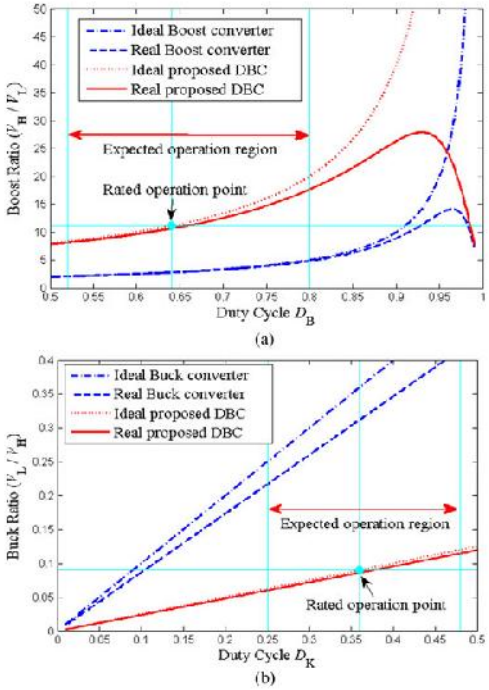

Fig. 14 Duty cycles versus voltage gain. (a) CCM boost operation.(b) CCM buck operation.

The ideal/real voltage ratio and the duty cycle of the proposed four-phase BDC, and the comparison curves with traditional boost or buck converters are sketched in Fig. 14. The worst-case ESRs of each inductor and capacitor are taken as 0.2 and 0.05 Ω, respectively. The expected operation region and the rated operation point are also given in the curves.

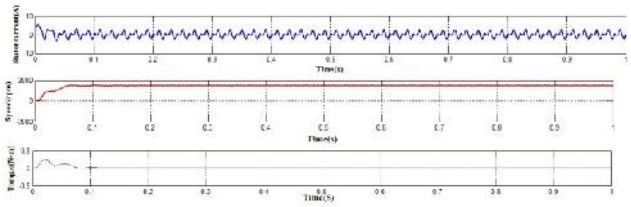

Fig. 14 Current, Speed, Torque Characteristics of the Induction motor

VI. CONCLUSION

This paper has proposed an interleaved high-conversion ratio step-up/step-down Bidirectional dc–dc converter fed induction motor drive applications. By using the capacitor charged in parallel and discharged in series by the coupled inductor, high conversion ratio and high efficiency have been achieved. The steady-state analyses of the proposed converter have been discussed in detail. The voltage gain and the utility rate of the magnetic core have been increased by using a coupled inductor with a low turn ratio. Hence the bidirectional DC-DC converter topology is suggested for motoring and regenerative braking. Here simulation of bidirectional dc-dc converter with R load was performed.Due to the active rectification in the secondary side of the transformer in the converter, overall efficiency increases. Both step up operation and the step down operation were done and then performed the motoring operation by integration the converter with the Induction motor drive.

REFERENCES

[1] X. Liu and B. Su, “Micro grids—An integration of renewable energy technologies,” in Proc. IEEE China Int. Conf. Electr. Distrib., Dec. 2008

[2] C.-H. Chang, et.al.,“Modularized bidirectional grid connected inverter with constant-frequency asynchronous sigma-delta modulation,” IEEE Trans. Ind. Electron., vol. 59, no. 11, pp. 4088, Nov-12.

[2] Wang, Yi-Feng, et al. "Interleaved High-Conversion-Ratio Bidirectional DC–DC Converter for Distributed Energy-Storage Systems—Circuit

Generation, Analysis, and Design." *IEEE Transactions on Power Electronics* 31.8 (2016): 5547-5561.

[3] D. Dong, I, et.al., "Grid-interface bidirectional converter for residential DC distribution systems—Part one: High-density two-stage topology," IEEE Trans. Ind. Electron., vol. 28, no. 4, pp. 1655–1666, Apr. 2013.

[4] B. G. Rawn, P. W. Lehn, and M. Maggiore, "Control methodology to mitigate the grid impact of wind turbines," IEEE Trans. Energy Convers., vol. 22, no. 2, pp. 431–438, Jun. 2007.

[5] J. Driesenet.al., "Distributed generation: Challenges and possible solutions," presented at the IEEE Power Engineering Society General Meeting, Montreal, QC, Canada, 2006.

[6] M. Black et.al,, "Value of bulk energy storage for managing wind power fluctuations," IEEE Trans. Energy Convers., vol. 22, pp.197, Mar. 2007.

[7] M. V.Krishna, et.al., "THD optimization of sequential switching technique based hybrid IPD modulation scheme for CMLI", *Science Engineering and Management Research (ICSEMR) 2014 International Conference*,pp. 1-7, 2014.